Aerosol Science and Technology
Publication details, including instructions for authors and subscription information:
http://www.informaworld.com/smpp/title~content=t713656376

Comparison of Experimental and Numerical Studies of the Performance Characteristics of a Pumped Counterflow Virtual Impactor

Gourihar Kulkarni[a]; Mikhail Pekour[a]; Armin Afchine[b]; Daniel M. Murphy[c]; Daniel J. Cziczo[a]
[a] Pacific Northwest National Laboratory, Atmospheric Science and Global Change Division, Richland, Washington, USA [b] Forschungszentrum Jülich GmbH, Institute for Chemistry and Dynamics of the Geosphere (ICG-1), Jülich, Germany [c] NOAA Earth System Research Laboratory, Chemical Sciences Division, Boulder, Colorado, USA

First published on: 03 January 2011

To cite this Article Kulkarni, Gourihar , Pekour, Mikhail , Afchine, Armin , Murphy, Daniel M. and Cziczo, Daniel J.(2011) 'Comparison of Experimental and Numerical Studies of the Performance Characteristics of a Pumped Counterflow Virtual Impactor', Aerosol Science and Technology, 45: 3, 382 — 392, First published on: 03 January 2011 (iFirst)
To link to this Article: DOI: 10.1080/02786826.2010.539291
URL: http://dx.doi.org/10.1080/02786826.2010.539291

Aerosol Science and Technology, 45:382–392, 2011

ISSN: 0278-6826 print / 1521-7388 online
DOI: 10.1080/02786826.2010.539291

Comparison of Experimental and Numerical Studies of the Performance Characteristics of a Pumped Counterflow Virtual Impactor

Gourihar Kulkarni,[1] Mikhail Pekour,[1] Armin Afchine,[2] Daniel M. Murphy,[3] and Daniel J. Cziczo[1]

[1]*Atmospheric Science and Global Change Division, Pacific Northwest National Laboratory, Richland, Washington, USA*

[2]*Forschungszentrum Jülich GmbH, Institute for Chemistry and Dynamics of the Geosphere (ICG-1), Jülich, Germany*

[3]*NOAA Earth System Research Laboratory, Chemical Sciences Division, Boulder, Colorado, USA*

Experiments and Computational Fluid Dynamic (CFD) simulations were performed to evaluate the performance characteristics of a Pumped Counterflow Virtual Impactor (PCVI). The diameter at which 50% of the particles were transmitted was determined for various flow configurations. Experimentally determined 50% cut sizes varied from 2.2 to 4.8 micrometers and CFD predicted diameters agreed within ±0.4 micrometers. Both experimental and CFD results showed similar transmission efficiency (TE) curves. CFD TE was always greater than experimental results, most likely due to impaction losses in fittings not included in the simulations. Ideal transmission, corresponding to 100% TE, was never realized in either case due to impaction losses and small-scale flow features such as eddies. Areas where CFD simulations showed such flow recirculation zones were also found to be the locations where particulate residue was deposited during experiments. CFD parametric tests showed that PCVI performance can be affected by the nozzle geometry and misalignment between the nozzle and collector orifice. We conclude that CFD can be used with confidence for counterflow virtual impactor (CVI) design. Modifications to improve the performance characteristics of the PCVI are suggested.

INTRODUCTION

The CVI is used in the atmospheric science community to separate interstitial (unactivated) aerosols from cloud elements so that the cloud elements can be analyzed. This separation is achieved by stopping and removing the gas phase and small particles but capturing large particles with sufficient inertia to cross gas streamlines. Particles with insufficient inertia to be captured follow the deflected streamlines and are removed from the system. Higher inertia particles are injected into a typically clean, dry and warm counterflow carrier gas that causes evaporation of condensed phase water. This technique has the advantage that a broad cut size range can be achieved by varying the flow rates associated with the CVI without changing the physical dimensions of the instrument.

Ogren et al. (1985) first described an aircraft CVI to separate cloud droplets from interstitial aerosols. Collected cloud droplets have also been evaporated and both off-line and in-situ chemical analysis methods used to examine the dissolved gases and non-volatile material (Noone et al. 1988a, b, 1990; Ogren et al. 1988; Twohy et al. 1997). Aircraft CVIs have also been used to separate ice crystals from interstitial aerosol particles (Noone et al. 1993; Field et al. 2001; Cziczo et al. 2004: Twohy and Poellot 2005; Wieprecht et al. 2005). After sublimation, residue material from the ice crystals was then analyzed for chemical composition. The CVI has also been employed using a wind tunnel to impart a relative motion to study surface fogs and clouds at field (Drewnick et al. 2007; Richardson et al. 2007) and laboratory (Schwarzenböck and Heintzenberg 2000; Noone et al. 1988b) sites.

Boulter et al. (2006) (hereafter B06) described a new CVI termed a Pumped Counterflow Virtual Impactor (PCVI) which uses a vacuum pump to produce a jet of air, replacing the relative velocity traditionally generated by aircraft flight or a wind tunnel. The authors investigated the performance characteristics, such as transmission and gas phase rejection efficiency, for various system conditions. B06 also identified limitations and uncertainties associated with the PCVI: imperfect transmission of particles, unexpected losses, and deviation of performance

Received 1 December 2009; accepted 18 October 2010.
Funding of this work was provided by the Pacific Northwest National Laboratory Aerosol and Climate Initiative and NOAA base funding. We wish to thank Karl Froyd for useful discussions.
Address correspondence to Gourihar Kulkarni, Atmospheric Science and Global Change Division, Pacific Northwest National Laboratory, 902 Battelle Blvd., Richland, Washington, 99354, USA. E-mail: Gourihar.Kulkarni@pnl.gov

at higher pressures. To date, these problems have not been resolved. This work uses flow modeling and new experiments to understand these observations and artifacts.

In the past, numerical techniques, i.e., computational fluid dynamics (CFD), have been used to understand the behavior of flow, particles, and the effects of various geometric configurations on CVI performance. Lin and Heintzenberg (1995) simulated an airborne CVI by using a three-dimensional mathematical flow model and the results were found to be in good agreement with the experimental data. Laucks and Twohy (1998) performed studies of an airborne CVI and calculated collection efficiencies of various size droplets which agreed well with data obtained during field studies.

Here we describe PCVI performance both numerically and experimentally. Results are compared for transmission efficiency (TE) characteristics and 50% cut size diameter for different flow conditions. For numerical analyses we employed the commercially available CFD software FLUENT 6.3 (2008). We have also performed additional parametric studies to understand the influence of design variables such as the throat length and focusing angle of the input nozzle and the effect of misalignment of nozzle and collection orifice on the performance characteristics of the PCVI.

EXPERIMENTAL

Figure 1 is a schematic diagram of the setup used for the experimental investigation of PCVI (Brechtel Manufacturing Inc, Berkeley, CA, USA) characteristics. Polydisperse ammonium sulfate aerosols ($\rho = 1730$ Kg m^{-3}) with sizes up to 10 micrometers were generated from a saturated solution using a simple nebulizer (Salter Labs 8900 Series Small Volume Jet Nebulizer). Filtered air at room temperature, $\sim$20°C, was used as the carrier gas. The aerosol stream was passed through a silica gel diffusion drier (TSI model 3062) to maintain a relative humidity below 35% and ensure crystalline aerosol (Cziczo et al. 1997). Flows through the PCVI were controlled using mass-flow controllers in output, add, and pump flow tubing; the input line flow rate was calculated as the balance. Particle transmission was found to be relatively insensitive to jet to orifice distance in B06, defined in subsequent sections, and this distance was therefore held constant at 1.8 mm. Pressure was monitored in 4 places: inside the PCVI and in inlet, outlet, and pump tubing. Total aerosol number density and size distribution of the test aerosol was monitored using CPCs (TSI model 3010) and LASAIR (Model 3001, 8 channels between 0.3 and 2.0 micrometers) and/or an Aerodynamic Particle Sizer (APS; TSI model 3021, 56 channels in the range of 0.5 and 20.0 micrometers), respectively. During all experimental measurements the APS was connected sequentially to inlet, outlet, and pump flow tubing to measure the particle size and number concentration. The CPC and LASAIR were connected in the same manner to monitor the total number concentration and size distribution. A flow splitter was connected upstream and downstream of the PCVI to allow these instruments to sample in parallel. The CPC 3010 has a lower detection limit of 10 nm diameter and the manufacturer's "best confidence" upper limit is 3 micrometers. The LASAIR was used for sizes less than 5 micrometers. The average number

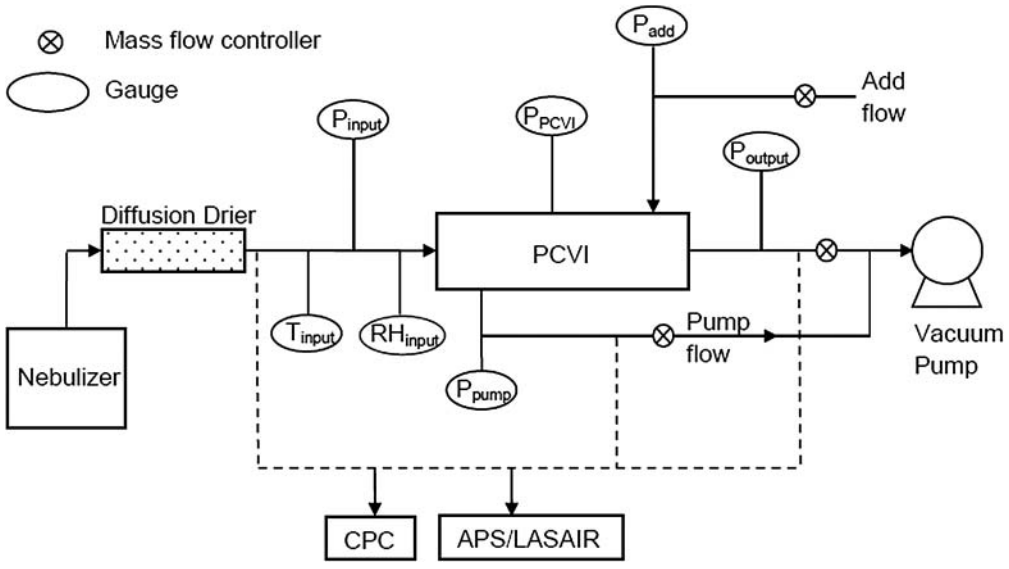

FIG. 1. PCVI experimental setup. The input tubing of the PCVI was connected to the aerosol generator system. The add flow splits inside the PCVI such that a fraction is directed with the input flow to the pump flow; this fraction is called the counterflow. The remainder of the add flow acts as the carrier gas of the output flow. The pump flow is therefore the combination of the counterflow and the input flow. During all experimental measurements the APS was connected sequentially to inlet, outlet, and pump flow tubing to measure particle number and size. The CPC and LASAIR were connected in the same manner to monitor the total number concentration and size distribution, respectively. The dotted line represents the tubing connections between the sampling ports of the setup and the three instruments (CPC, APS, and LASAIR).

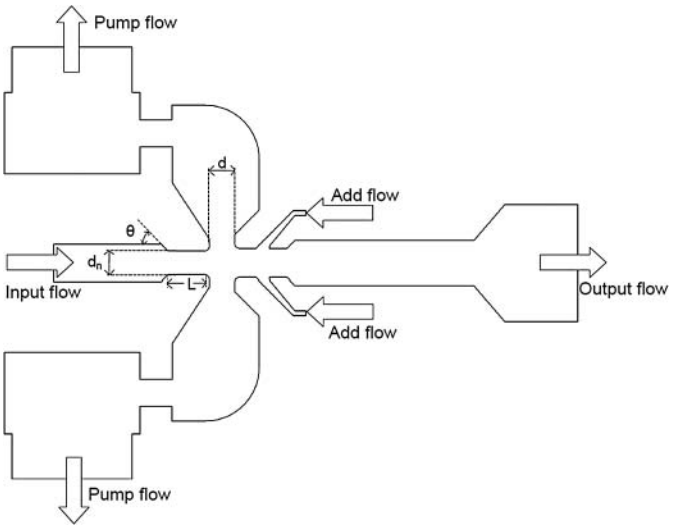

FIG. 2. Schematic diagram of the CFD simulated PCVI geometry showing important dimensions and flow boundary conditions. The design parameters of the acceleration nozzle are the diameter (d_n), the converging angle (θ), and the length (L). The respective values used were 1.3716 mm, 45 deg, and 2.4384 mm. The distance (d) between the nozzle and collector orifice was set at 1.8 mm.

concentration of particles upstream of the PCVI varied between 4×10^3 and 9×10^3 per cm^3.

The cross section of the PCVI with critical dimensions noted is shown in Figure 2. The inlet polydisperse aerosol stream is termed the input flow, which enters the apparatus through the acceleration nozzle. A particle-free gas flow, termed the add flow, must be greater than the output flow. It splits into the counterflow (flows in the opposite direction to the input flow) and the output flow. The counterflow joins the input flow and the combination is termed the pump flow. For more details refer to B06. By controlling add and input flows variable 50% cut size diameters can be obtained.

The PCVI transmission efficiency, defined as the ratio of particle number in the output flow to particle number in the input as a function of particle aerodynamic diameter, was measured for a variety of flow conditions. An advantage of determination of TE is that it does not depend on absolute concentration. Note that by defining transmission efficiency in terms of relative particle number rather than relative particle concentration the flow ratio between the inlet and outlet is automatically included. The 50% cut size diameter, the particle size at which 50% of incoming particles were transmitted into the output flow, was determined from the collection efficiency curves. Table 1 presents the calculated 50% cut size diameter and measured pressures under the various flow conditions. The counterflow rate was calculated as:

$$F_{counterflow} = F_{addflow} - F_{output} \quad [1]$$

where $F_{output} = 1.0$ lpm and was kept constant in all experiments.

NUMERICAL MODELING

The majority of numerical modeling of the PCVI was done at the Pacific Northwest National Laboratory (PNNL) using the commercial CFD software FLUENT (Ver. 6.3, ANSYS). FLUENT solves conservation equations for mass, energy, and momentum to calculate flow properties (e.g., velocity profiles for various flow configurations). Three-dimensional simulations were utilized for this work.

The FLUENT pre-processor software GAMBIT (Ver. 6.3, ANSYS) was used to build the physical, or "mesh," model for

TABLE 1
Comparison of experimental to CFD 50% cut size diameters (in micrometers) and Stokes number (sqrt(Stk_{50})) for various flow (F) and pressure (P) configurations. For detailed Stokes calculation procedure refer to B06. The subscript indicates the location within the PCVI at which the measurement was made (see Figure 1 for details). The corresponding TE curves for the cases in bold are shown in Figure 4b

Case number	F_{input} (lpm)	$F_{counterflow}$ (lpm)	P_{input} (mbar)	P_{PCVI} (mbar)	P_{output} (mbar)	50% cut size		sqrt(Stk_{50})	
						Expt.	CFD	Expt.	CFD
1	**11.97**	**1.82**	**998**	**755**	**992**	**2.24**	**2.18**	**2.31**	**2.23**
2	9.64	1.82	998	853	993	2.68	2.52	2.45	2.30
3	9.20	1.82	998	868	993	3.09	3.10	2.76	2.77
4	8.60	4.32	997	885	992	3.77	4.05	3.25	3.50
5	**6.90**	**1.32**	**997**	**928**	**995**	**3.21**	**2.81**	**2.48**	**2.18**
6	6.88	1.82	997	928	997	3.42	3.45	2.64	2.67
7	6.78	1.62	997	930	997	3.40	3.40	2.61	2.61
8	6.70	2.82	997	932	994	4.05	4.30	3.08	3.27
9	**6.60**	**3.82**	**997**	**933**	**993**	**4.81**	**4.80**	**3.63**	**3.63**
10	6.50	3.32	997	935	994	4.65	4.78	3.49	3.58

the PCVI domain (Figure 2). Approximately 6×10^5 cells with variable mesh density were used. Relatively higher mesh density was used for the areas with rapid changes of dependent variables (e.g., velocity, pressure) to make use of computing power most efficiently. To reduce the computational time the lengths of add and input flow tubing were shortened after verification that this simplification did not change the flow characteristics or the 50% cut size diameters. We did not simulate the complex fittings used for particle number and size measurements located both upstream and downstream of the PCVI.

To capture the boundary layer shear flow, which is important when solving for turbulence, a non-dimensional distance is defined as $y^+ = \rho u_T y/\mu . u_T = \sqrt{T_w/\rho}$ is the friction velocity with T_w being the wall shear stress. ρ and μ are the fluid's density and dynamic viscosity, respectively. The distance y^+ was set to unity (FLUENT 6.3 2008) and the distance (y) from the centroid of the first mesh element to the wall was calculated. Grid independence tests were performed to confirm the mesh density did not affect the final solution.

Boundary conditions were assigned for the solution of the fluid motion. These included the input, output and add flows of the PCVI as "mass flow inlet" and pump flow as "pressure outlet" conditions. The boundary conditions are initialized using the experimental values tabulated in Table 1 for each case. Table 2 provides the solution settings for FLUENT applicable to this study. A renormalization group theory (RNG) based on the turbulent kinetic energy (κ) and its dissipation rate (ε), commonly termed a RNG $\kappa - \varepsilon$ turbulence model, was employed to account for turbulence effects. Turbulence parameters such as turbulence intensity (TI) and turbulence viscosity ratio (TR) were imposed on the flow boundary values. TI is calculated as:

$$TI = 0.16\,(\mathrm{Re})^{(-1/8)} \qquad [2]$$

where Re is the Reynolds number, calculated as:

$$Re = (\rho U d_n)/\mu \qquad [3]$$

TABLE 2
FLUENT settings used for flow modeling

Solution parameters/ boundary conditions	Settings
Solver	Three dimension double precision, pressure based Navier stokes equation, steady state, implicit and absolute velocity formulation, energy and viscous heating enabled, species transport, RNG $\kappa - \varepsilon$
Pressure calculation	Standard
Pressure-velocity coupling	SIMPLE
Momentum and energy	Second order upwind

where ρ is the air density, U is the mean velocity at the inlet nozzle exit plane, d_n is the diameter of the acceleration nozzle, and μ is the dynamic viscosity of the air. For various input flow rates Re varied from 4000 to 7500. For most model runs TI was varied between 5 and 10%. TR was defined as the ratio of turbulent viscosity to the molecular dynamic viscosity and a ratio from 5 to 10 was used in the simulations.

The FLUENT "discrete phase model" was used to understand how particle trajectory was influenced by the PCVI flow characteristics. This model calculates the trajectories of individual particles in the gas phase. The effects of turbulence were included by enabling a stochastic tracking (random walk) model which includes the effects of instantaneous turbulent velocity fluctuations. Injected particles were modeled as spheres with density equal to crystalline ammonium sulfate. Particles with variable diameter were introduced at the input boundary of the PCVI with a velocity equivalent to that of the gas entering the inlet. The PCVI walls where eddies and vortices were observed were set as "escapes" (meaning lost) and all other regions set to "reflect" (meaning elastic bouncing) boundary conditions.

Sets of ~150 particles of each size were launched from the input boundary condition. Sensitivity studies of launching larger particle numbers (up to ~600) did not change the TE characteristics. The solutions were obtained using an 'uncoupled approach' which means the fluid flow field is allowed to act on the particles but not vice versa. The assumption is valid for low number densities of small spherical particles (~10 micrometers) used in the current simulations. FLUENT calculates the turbulent dispersion of particles using the instantaneous fluid velocity (summation of average and fluctuating gas flow velocity) along the particle path (FLUENT 6.3 2008).

The time a particle spends in turbulent motion along the particle path before being transported into another eddy is called the Lagrangian integral time and is approximated by $T_L = C_L(\kappa/\varepsilon)$ where C_L is a time scale constant. The time T_L is determined by the particle inertia. For the range of particle sizes considered in this study C_L was 0.15 (FLUENT 6.3 2008). The sensitivity of C_L was checked by varying the value from 0.05 to 0.20; no variation was observed at the 50% cut size diameters in any simulation. Another important turbulent variable is the eddy lifetime (T_e). It can be defined either as a constant $T_e = 2\ T_L$ or as a random variation $T_e = -\ T_L \log(r)$, where r is a random number between 0 and 1. To maintain the consistency across the simulations (cases 1 to 10) constant T_e option was used. To test the validity of the turbulent parameters the 50% cut size diameters from CFD and experiments were compared (Table 1). An agreement within ± 0.4 micrometers was observed.

A transport model with water vapor, nitrogen and oxygen was used to describe the sub-saturated gas flow. The model simulations were run until the residuals (difference between the current and previous iteration values of dependent variables) were less than 10^{-6}. In addition, the mass flow rate surface integrals calculated from the imposed boundary conditions were used to check for solution convergence and the final solution was

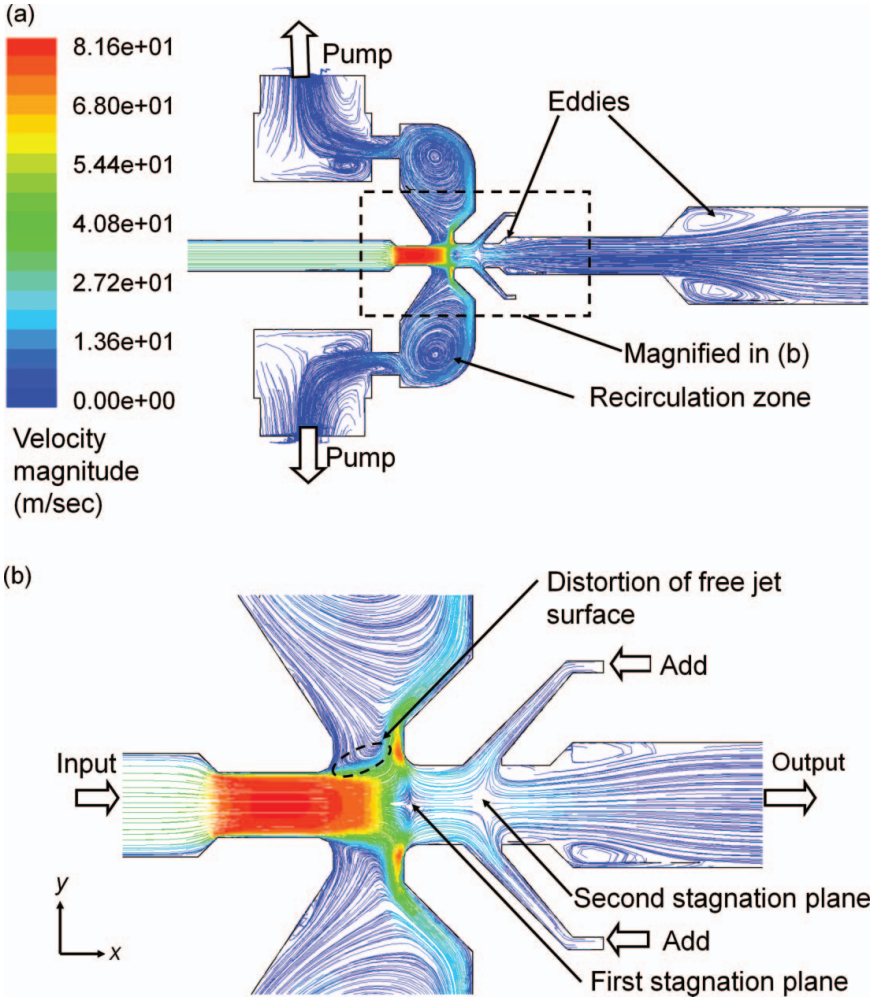

FIG. 3. Fluid flow velocity characteristics during passage through the PCVI. (a) The domain of the PCVI that was analyzed numerically. For critical dimensions please refer to Figure 2. The domain shows the boundary conditions and the eddies and recirculation vortices generated as a result of the complex geometry. (b) Magnified section from (a).

checked against the grid independence (i.e., the solution could not be further improved by increasing the mesh size). For the final solutions TE was determined as the ratio of the number of particle trajectories that intersected the output flow to the total number of particle trajectories that were initiated at the input flow boundary.

CFD simulations allow detailed insight into small-scale flow patterns including the location of features such as eddies, recirculation zones, wall-flow separation regions, and so on. Figure 3a shows an example of an internal PCVI flow pattern. A magnified view of the region near the nozzle and collection orifice is shown in Figure 3b. The two stagnation planes (a plane where longitudinal velocity is zero) typically developed in a CVI are noted. The detailed flow picture shows that these planes are slightly convex with the shape determined by the ratio of the input flow and counterflow. The distance between the planes is the distance that a particle must travel against the counterflow to reach the output flow (i.e., this is the inertial barrier a particle must overcome to be transmitted through a CVI). The streamlines from the input nozzle meet the counterflow streamlines at the first stagnation plane. The second stagnation plane is developed from the splitting of the add flow into the counterflow and output flow. The nozzle parameters of throat length (L) and focusing angle (θ) are shown.

The PCVI was also independently modeled by Forschungszentrum Jülich GmbH using ANSYS CFX version 11 (2008). The mesh included approximately 2.5 million nodes. The flow field was calculated by solving the Navier-Stokes equations for a steady state, compressible, and turbulent flow. The Shear Stress Transport (SST) k-w based turbulence model was used. Particle trajectories were calculated using the Schiller-Naumann drag force model and turbulent dispersion in regions where the turbulent viscosity ratio was above the value 5. Particles were assumed to be sufficiently dilute to not affect the flow field and to be lost upon wall collision with no bounce. Other flow settings are shown in Table 3. Additional figures

TABLE 3
CFX settings used for flow modeling

Solution parameters	Settings
Boundary conditions	All boundaries are mass flow controlled. At the inlet the turbulence is set to low intensity 1%.
Solver	Three dimensional flow model, pressure based Navier stokes equation, steady state, compressible, Shear Stress Transport $\kappa - \omega$ turbulence model.(SST). Heat transfer is set to total energy including the viscous work term.
Particle calculation	One-Way coupling, drag force is Schiller-Naumann, turbulent dissipation force in regions, where the eddy viscosity ratio is greater than 5. Perpendicular coefficient is zero at all walls.
Advection scheme	Second order

from the Jülich CFX modeling results are available at http://www.esrl.noaa.gov/csd/groups/csd2/techref/. Except as noted, results in this paper are from the PNNL modeling.

RESULTS AND DISCUSSION

Transmission Efficiency

Figure 4a is an idealized TE curve (i.e., TE versus diameter) observed in experimental and CFD studies. There is an increase from non-transmitted particles through the 50% cut size and then up to maximum efficiency (Zone I), a gradual decrease to a local minimum (Zone II), followed by a region of constant or slightly increasing transmission (Zone III). The TE for three different flow configurations (highlighted in Table 1) are used in the current analysis shown in Figure 4b. We highlight these cases for three main reasons: extreme and distinct 50% cut sizes, TE curves that can be individually analyzed and co-plotting them allows us to understand the relative relationship between the curves. The experimentally determined and CFD calculated 50% cut sizes and Stokes diameters all agree within ± 0.4 micrometers diameter. The corresponding 50% cut size diameter square roots of the Stokes number are also shown in Table 1. Uncertainty in the size of the inlet orifice in B06 does not allow for a direct comparison to those values. Figure 4b also shows that both experimentally and numerically determined TE values do not reach 100%, implying an imperfect transmission of particles. The experimental maximum TE values are observed to be lower than the numerical simulations in all three cases.

More systematic CFD simulations were performed in considering the application of the PCVI to atmospheric sampling studies (Cziczo et al. 2004; Gallavardin et al. 2008). In these studies the input and output flow rates through the PCVI are usually fixed, whereas the add flow is varied to "set" the 50% cut size. The 50% cut size for various add flows and three types (ice, ammonium sulfate, and dust) of aerosol particles are calculated as shown in Figure 5a. It can be seen that with increase in add flow (or indirectly the counterflow) the cut size increases. The aerodynamic diameter calculations show a similar trend of increase in cut size with increase in add flow. Also shown (Figure 5b) are the comparison between the CFD and experimental 50% cut sizes for ammonium sulfate aerosol particles. In this study both the counterflow and input flow rates were varied. It is observed that the cut sizes from CFD and experiments agree within 0.7 micrometers. The broader agreement when compared with the Table 1 results may be attributed to the sensitivity of CFD model parameters to flow configurations such as shown in Figure 5b. It can be further observed that for different flow ratio (0.28 and 0.33) it is possible to obtain similar 50% cut size (3.0 micrometers), and increase in flow ratio does not always yield higher 50% cut size. Therefore flow ratio alone cannot be used as a single parameter to predict the 50% cut size diameter.

To help understand the shape of the transmission curve, Figure 6a is used to show the trajectories of single particles injected from the same coordinates of the input boundary condition. The influence of the stochastic turbulence model can be observed in that their trajectories are not identical. The diameters of these six particles are identical and near the 50% cut size diameter for the conditions. The length of the vectors shown in the figure represents velocity magnitude. It is observed that the counterflow is not uniformly developed so that the velocity near the wall is larger than the magnitudes at the centerline. The particle nearest the wall (trajectory 1) experiences the highest drag, is stopped and turned so that it is ultimately pumped away. Particles on trajectories 2 through 4 experience the least drag and enter the output flow. Particle trajectories 5 and 6 intercept the counterflow at an angle since they pass through an eddy and subsequently bounce off the wall. Elastic collisions in this simulation ultimately allow these particles to enter the output flow but it is noteworthy that a real particle may undergo processes such as sticking or breakup that lead to rejection. Thus, particles are shown here to be captured or rejected based on their location in the flow independent of their size and mass. This is the physical reason for the non-step function transmission at a distinct cut size shown in Figure 4. Figure 6b shows the variation in particle size that can be transmitted for the counterflow velocity distribution shown in Figure 6a. It is observed that the size of transmitted particles increases from the central core region (radius = 0) toward the wall (radius = 1).

There are two reasons that a perfect 100% TE is not realized regardless of particle size in either the experiments or simulations. First, the flow fields shown in Figures 3 and 6 illustrate that particles moving along the streamlines farthest from the nozzle axis (in the wall boundary layer) are deflected at the free

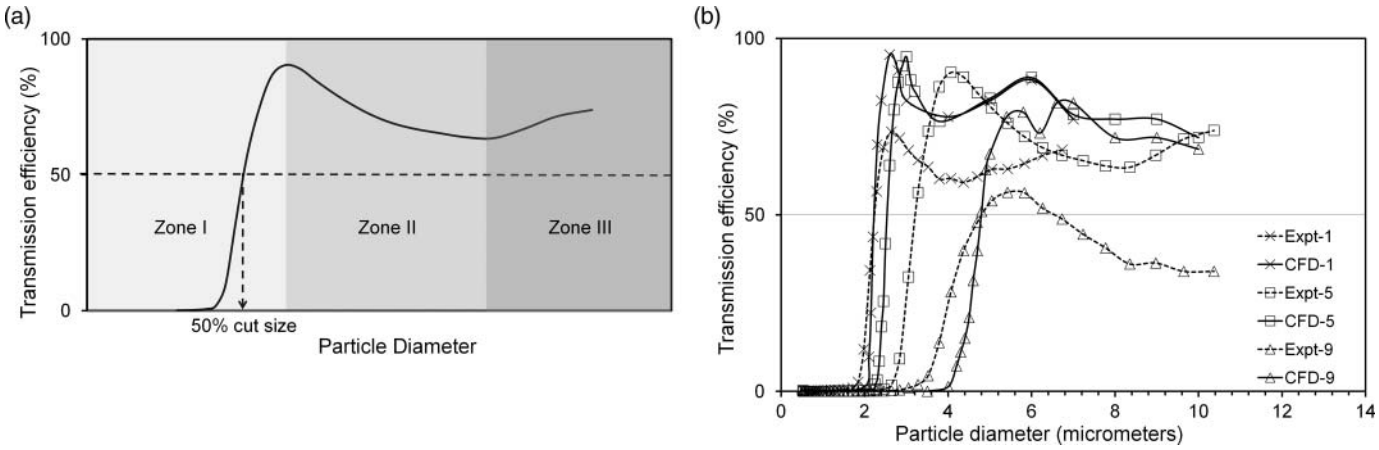

FIG. 4. (a) Idealized transmission efficiency (TE) curve features. Zone I is the region where TE transitions from rejected particles to the maximum. In Zone II the TE decreases and reaches local minimum. In Zone III the TE remains flat or increases slightly. The smallest diameter at which 50% transmission occurs is the 50% cut size diameter. (b) Comparison of experimental (Expt) to CFD TE for Case numbers 1, 5, and 9 (Table 1).

surface of the jet as it leaves the nozzle and become trapped inside recirculation vortices (Figure 3b) to join the pump flow. In addition to the axially dependent drag, the distortion of this free jet surface makes it impossible to achieve 100% TE for the particles sizes considered here. Approximately 15 to 25% of particles losses occur within this region depending upon the particle size. Second, particles are also observed both experimentally (in the form of ammonium sulfate residue) and numerically (in the form of surface contact) to impact the region where the inlet is reduced in diameter as it enters the PCVI (Figure 3).

The CFD simulations also allow possible explanation for the morphology of Zones I, II, and III (a maximum TE followed by a local minimum followed by stable or slightly rising TE). In Zone I the particles are observed to follow the streamlines as a function of their mass (i.e., diameter for these constant density simulations). Particle sizes at the end of Zone I where maximum TE was observed are best collimated near the centerline. This results in the smallest particles which are transmitted being less likely to impact in the region where the inlet diameter is reduced. Furthermore, these small transmitted particles are more likely to be moved away from downstream wall turbulences. More massive particles (Zone II) are not as tightly collimated and relatively more are either impacted in the inlet or experience higher drag and/or turbulence such that they are unable to pass through the stagnation planes. This leads to decrease in the TE. We also observed a crossing trajectory phenomenon (Hu and McFarland 2008; Hari et al. 2007) where the particles from one side of the nozzle cross the mid plane and impact on the opposite-side wall. Particle losses within the nozzle could also contribute to the decrease in the TE. As mass increases further the increased drag near the walls and/or minor turbulence is insufficient to stop a particle so a high fraction are collected in the output flow line; this is likely the reason for some TE 'recovery' in Zone III.

Although the morphology of transmission is similar between the experimental and numerical results there are differences in the absolute TE. These differences could be attributed to the limitations of the CFD modeling where it is not possible to simulate the experimental set up (for example we do not simulate the upstream and downstream fittings) and the particle losses at various regions inside the PCVI. In all cases the numerical simulations indicated a higher maximum TE than the experiments. It is noteworthy that although the particle measurements were made as close to the PCVI as possible, residual ammonium sulfate was observed on all intermediate fittings. This is likely a result of both the impaction of large particles as described in the last paragraphs as well as the development of small-scale turbulence within the fittings. Neither of these processes is modeled in the simulation field and both lead to reduced TE in the experimental relative to the CFD results.

Characterization of Pump and Output Flow

Observing the flow configuration in Figure 3 it is reasonable to consider measurements of rejected particle properties in the pump flow line. In a situation where cloud sampling is occurring, for example, one could consider comparison of residuals in the sample flow to unactivated aerosols in the pump flow.

Experimental and CFD characterization of the pump flow was performed. Experimentally, a size distribution was measured in the pump flow for Case 7 in Table 1. It was observed that the TE of 2 micrometer diameter particles (i.e., particles lower than the 50% cut size) was 15%. A CFD simulation of the same case was performed. Particles of 2 micrometer diameter were introduced at the input boundary condition with 28% leaving the pump flow boundary (i.e., the remainder were lost due to wall impaction). The lower TE for experimental versus CFD can again be explained by the presence of fittings and tubing used for physical measurements which are not included in the

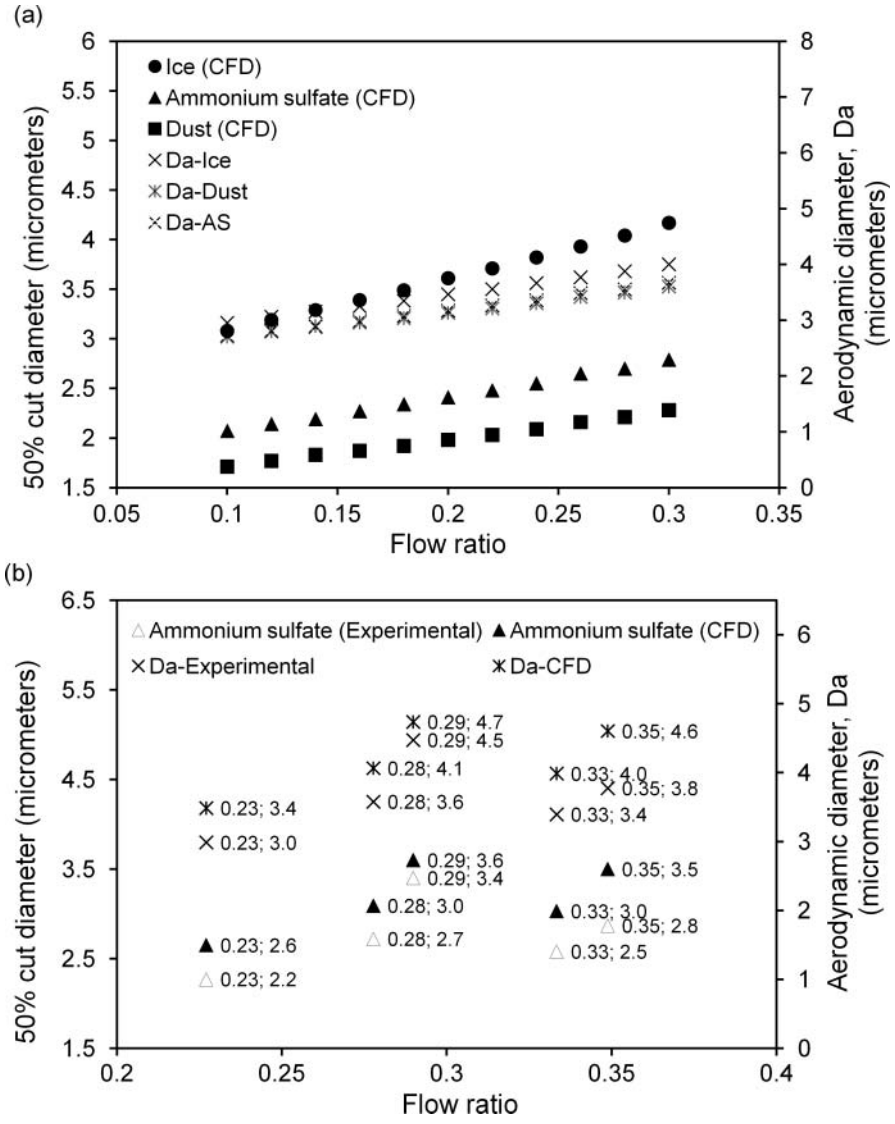

FIG. 5. CFD and experimentally determined 50% cut size aerosol diameters for various counterflow to input flow ratios. (a) The input flow was kept constant and counterflow was varied. The data shows an increase in the 50% cut size and aerodynamic diameter (Da) with increase in the flow ratio. (b) Both counterflow and input flow were varied in experiments and corresponding simulations. See text for more detailed discussion about flow ratio. The data labels shows the flow ratio and 50% cut size diameter (in micrometers) respectively with agreement within 0.7 micrometers. For all studies the density of ice, ammonium sulfate and dust aerosols assumed were 920, 1730, and 2500 kg/m^3, respectively.

model. It is noteworthy that the location of impaction in the CFD simulation (regions of high vorticity or where significant flow recirculation occurs) correlated with observed particle deposits in the PCVI. Experiments also showed that particles larger than the cut size diameter (i.e., those that were not able to enter the sample flow due to the aforementioned reasons) were found in the pump flow.

Particle behavior in the output flow was specifically investigated using CFX. Figure 7 shows trajectories of 5 micrometer diameter particles. For these flow conditions the transmitted particles are concentrated in a small portion of the output flow. The curvature of the particle tracks is due to the recirculation of the flow in the output region with the eddies redirecting the particles leading to radial asymmetry in concentration. Since the eddies are likely to be unsteady, the result is that the transmitted particles would be concentrated in varying spots in the output flow. This would lead to difficulties in sampling a portion of the output flow, as found experimentally by B06. In the CFX model results, the non-uniformity in the outlet flow decreased at a higher flow rate, evidently due to turbulent mixing in the output flow.

In conclusion, attempts to sample particles below a CVI cut size in a pump flow should be attempted with care. Impaction losses are significant and may be biased by properties such as particle phase and shape (i.e., particles which are not lost due to impaction may not be representative of the whole). Furthermore,

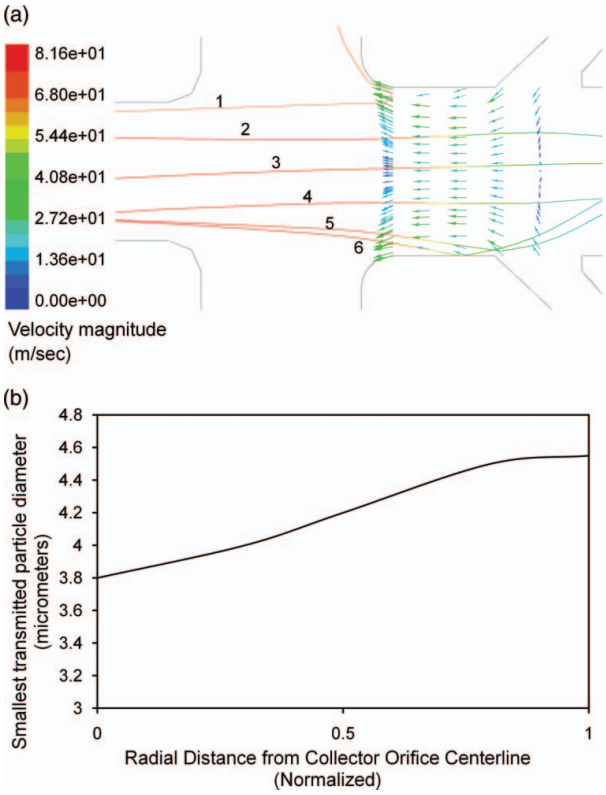

FIG. 6. (a) Velocity vector distribution inside the collector orifice. Trajectories 1 through 6 represent identically sized particles at different axial locations. The particle in trajectory 1 experiences the highest drag, is stopped and turned for removal in the pump flow. Trajectories 2 through 6 experience less drag and are able to join the sample (output) flow although particles 5 and 6 experience a surface impact. (b) The variation in smallest transmitted particle diameter as a function of normalized radial distance from the centerline.

under some flow conditions the transmitted particles are not uniformly mixed in the outlet flow. A mixing chamber or similar technique may be required for measuring quantitative particle concentrations.

Alignment Effects

One possible source of reduced TE is imperfect alignment of the PCVI either after construction or upon reassembly after cleaning. Two sets of numerical simulations were performed to quantify possible errors. First, the inlet and collection orifice were displaced axially. Second, the inlet was angularly misaligned with the remainder of the PCVI. These studies are referred as the axial and angular misalignment studies respectively.

The CFD simulations with axial misalignment of 0.5 mm were performed using the Case 1 flow configuration from Table 1. The simulations produced asymmetric and turbulent flow with eddies and vortices as shown in Figure 8a. This led to particles losses and the effect was simulated by assigning these turbulent flow region walls to 'particle trap' boundary conditions. The effect of misalignment on TE is shown in Figure 8b. It is observed that the maximum TE reached is approximately 45% and the TE curve features are identical to those shown Figure 4a. Similar results are observed with angular misalignment of 1.5 deg inclination. Both the magnitude and curve features became more pronounced in the 3.0 and 5.0 deg misalignment simulations. It should be noted that the magnitude of these misalignments are likely to be unrealistic in the actual assembly of the PCVI and should be considered an upper bound for what is physically possible For this reason we were not able to experimentally validate 'particle trap' boundary condition (i.e., verify

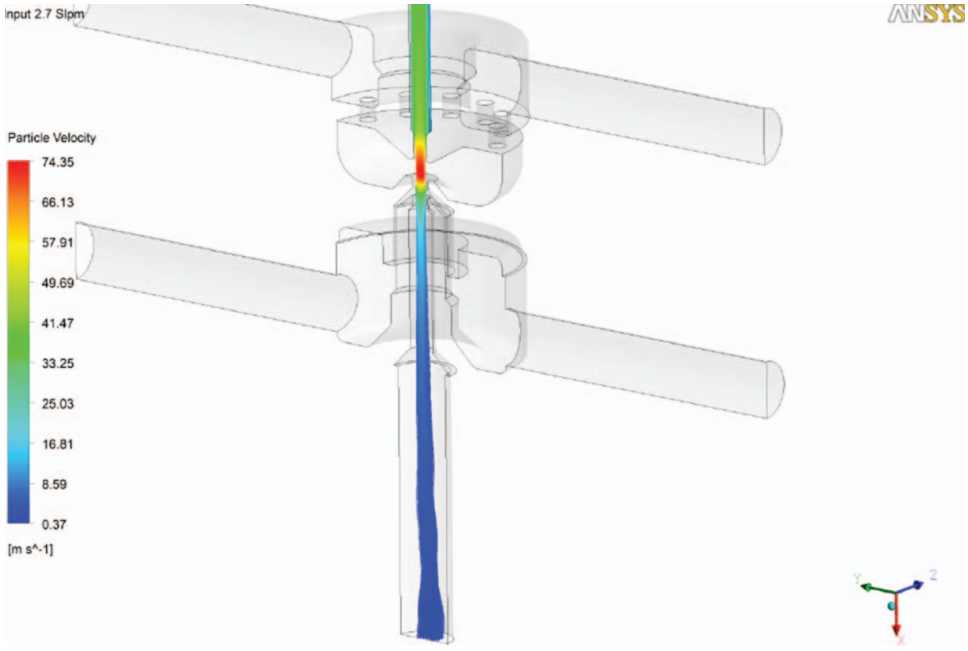

FIG. 7. CFD (CFX software) simulated particle trajectories for 5 micrometer diameter particles that reach the output sampling port. The non-linear nature of the particle trajectories is due to eddies in the output region resulting in inconsistent radial transmission. See text for further details.

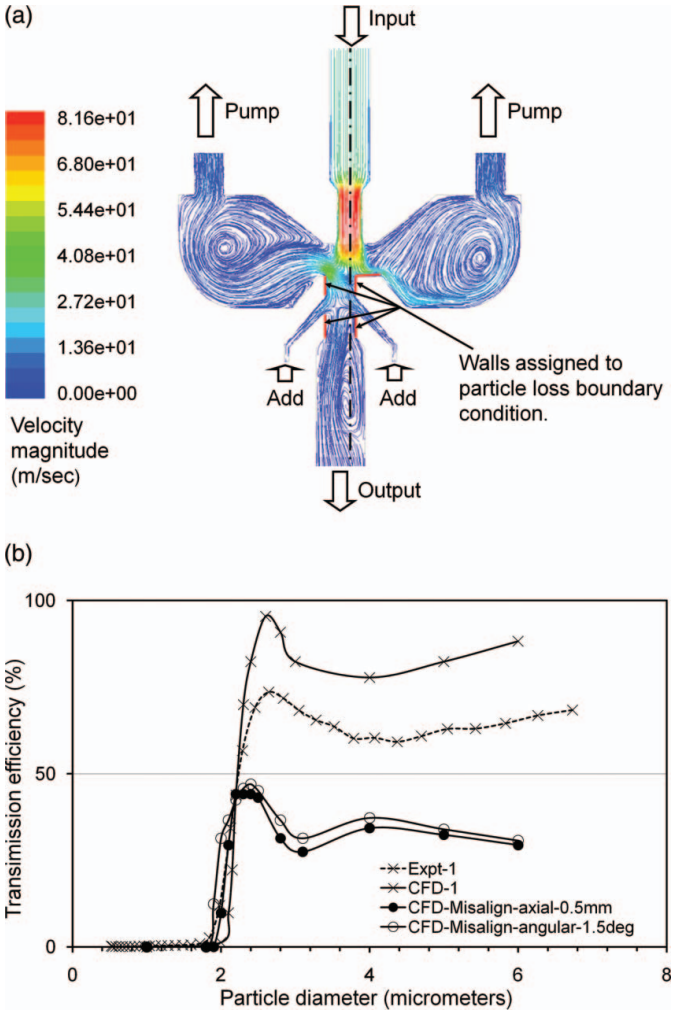

FIG. 8. (a) Velocity magnitude pathlines when the PCVI is axially misaligned/offset by 0.5 mm. Asymmetric and turbulent flows might lead to particles losses inside the PCVI which are modeled by using particle loss boundary conditions. (b) The effect of axial and angular misalignment on the transmission efficiency. Experimental (Expt) and model (CFD) Case 1 are compared to two misalignment cases (see text for details).

if particles which impact a wall are invariably lost) although the aforementioned observations without misalignment of residual material in locations where eddies or vortices where predicted support this contention.

Nozzle Geometry Effects

CFD simulations were also performed to study the effect of the inlet nozzle length (L), convergence angle (θ) and the combination of length and focusing angle on PCVI performance characteristics. In the first study the inlet was modified to 2.5 times the original length L. Second, the effect of changing θ from 45 to 30 deg was investigated. Third, changes to a nozzle length 2.5 times L and θ of 30 deg. were combined. CFD transmission curves are compared to the control simulation and experiment for Case 1 (nominal L and θ) in Figure 9.

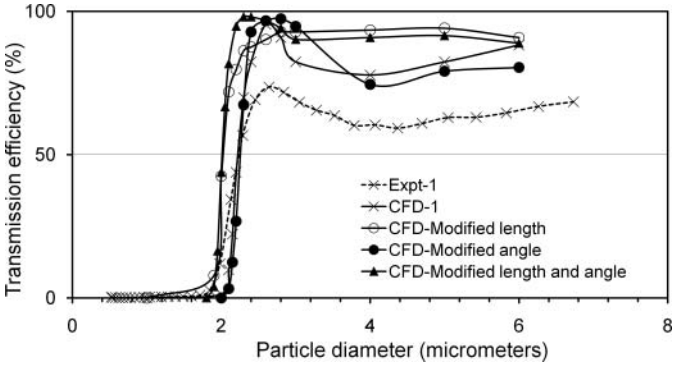

FIG. 9. The effect of modified nozzle length, focusing angle and combined modified length and focusing angle on the transmission efficiency. Experimental (Expt) and model (CFD) Case 1 are given for comparison (see text for details).

In the case where L is extended by a factor of 2.5 the CFD simulations show that the 50% cut size diameter is moved to a smaller size and the TE peak is lower. In the case where the convergence angle is less severe neither the cut size diameter nor the TE peak is observed to change but the average transmission in the region around the peak is higher. In the case where both L is extended and θ is less severe the cut size diameter is smaller while the TE peak and the average transmission in the region of the peak remain high.

CFD simulations show that the average particle velocity, which was calculated at the central axis of the nozzle exit from three cases (1, 5, and 9), is higher after the inlet orifice in the case where L is extended by a factor of 2.5. Smaller particles therefore have sufficient inertia to penetrate to the sample flow and the result is the lower average cut size observed when extended length is used. In the case where the convergence angle is less severe the CFD simulations show that less particle impaction occurs at the input nozzle, resulting in the higher average TE around the maximum. In the case where L is lengthened and θ is less severe the result is that the cut size is lower due to higher particle velocity ($\sim$10% higher) and particles are less likely to impact at the input nozzle. Furthermore, because velocities of higher particles are less likely to become entrained in the eddies developed near the free jet surface where the collector orifice meets the pump flow.

SUMMARY AND CONCLUSIONS

PCVI performance was evaluated using both experimental and CFD techniques. Agreement within $\pm$0.4 micrometers for 50% cut-size and Stokes diameters was obtained between the experimental and CFD data. Systematic studies showed that various 50% cut sizes can be obtained by varying the counterflow while keeping the input flow constant. Particle TE curve characteristics were found to be similar for both approaches but absolute particle transmission and the efficiency at larger sizes were different, most likely due to fittings present in the experimental setup which were not modeled. This resulted in consistently lower experimental TE when compared to CFD values. Misalignment simulation showed significant a decrease

in TE and an increase in eddies and vortices of various scales. The misalignments simulated here are more extreme than could be physically replicated with the PCVI and are thus considered unlikely to occur in field or laboratory measurement.

CFD evaluation performed on the nozzle geometry showed that neither increasing the nozzle throat not decreasing the focusing angle of the particles significantly improved the performance but the combination of these led to both a sharp cut size and improved TE. New nozzle geometry designs are suggested.

Numerical studies indicated wall impaction loss on the order of 25% and 10% inside the nozzle and output flow domain, respectively. Furthermore, the location of eddies in the simulation are consistent with observed particle deposit locations during experiments. For these reasons we believe CFD analysis can be used with confidence to understand the performance characteristics of CVI designs.

Based upon our analysis of the PCVI performance characteristics five aspects of the B06 PCVI geometry should be improved and we intend to use the CFD software to achieve them:

1. The nozzle free jet surface was affected by the eddies developed within the PCVI. Significant particle losses were observed in this region. Redesign of this region should minimize the losses, which would also lead to increased TE.
2. A non-uniform counterflow velocity distribution was observed which caused transmission of variable particle size across the collector orifice. Redesign of the geometry (diameter and length) should minimize variability across the collector orifice.
3. Performance characteristics are sensitive to the nozzle dimensions L and θ. The results show that extended length and less severe angle reduce flow irregularities and impaction in the inlet thereby leading to increased TE.
4. Particles in the PCVI output flow are not symmetric with respect to radius due to the presence of eddies after the collection orifice. Depending on sampling method a mixing chamber or similar technique may be required to collect and analyze a representative sample of separated particles.
5. There are very large particle losses in the pump flow, probably preventing quantitative sampling of particles below the cut point that are carried in the pump flow. We note that these simulations have been restricted to spherical particles. Some hydrometeors, namely ice crystals, are of interest for CVI research but are usually non-spherical. After above studies have been carried out the future research will attempt to elucidate the inertial separation of such complex shapes as well as the effect of processes such as breakup and impaction (i.e., shatter) on subsequent analytical techniques.

REFERENCES

Boulter, J. E., Cziczo, D. J., Middlebrook, A. M., Thomson, D. S., and Murphy, D. M. (2006). Design and Performance of a Pumped Counterflow Virtual Impactor. *Aerosol Sci. Technol*. 40:969–976.

CFX v.11. (2008). ANSYS Inc, Canonburg, PA, USA.

Cziczo, D. J., Nowak, J. B., Hu, J. H., and Abbatt, J. P. D. (1997). Infrared Spectroscopy of Model Tropospheric Aerosols as a Function of Relative Humidity: Observation of Deliquescence and Crystallization. *J. Geophys. Res.* 102:18843–18850.

Cziczo, D. J., Murphy, D. M., Hudson, P. K., and Thomson, D. S. (2004). Single Particle Measurements of the Chemical Composition of Cirrus Ice Residue During CRYSTAL-FACE. *J. Geophys. Res.* 109. doi:10.1029/2003JD004032.

Drewnick, F., Schneider, J., Hings, S. S., Hock, N., Noone, K., Targino, A., Weimer, S., and Borrmann, S. (2007). Measurement of Ambient Interstitial and Residual Aerosol Particles on a Mountaintop Site in Central Sweden Using an Aerosol Mass Spectrometer and a CVI. *J. Atmos. Chem.* 56: 1–20.

FLUENT 6.3. (2008). ANSYS Inc, Canonsburg, PA, USA.

Field, P. R., Cotton, R. J., Johnson, D., Noone, K., Glantz, P., Kaye, P. H., Hirst, E., Greenaway, R. S., Jost, C., Gabriel, R., Reiner, T., Andreae, M., Saunders, C. P. R., Archer, A., Choularton, T., Smith, M., Brooks, B., Hoell, C., Bandy, B., and Hemysfield, A. (2001). Ice Nucleation in Orographic Wave Clouds: Measurements made During INTACC. *Q. J. Roy. Meteorol. Soc.* 127:1493–1512.

Gallavardin, S. J., Froyd, K. D., Lohmann, U., MÖehler, O., and Cziczo, D. (2008). Single Particle Laser Mass Spectrometry Applied to Differential Ice Nucleation Experiments at the AIDA Chamber. *Aerosol Sci. Technol.* 42:773–791.

Hari, S., McFarland, A. R., and Hassan, Y. A. (2007). CFD Study on the Effects of the Large Particle Crossing Trajectory Phenomenon on Virtual Impactor Performance. *Aerosol Sci. Technol.* 41:1040–1048.

Hu, S. and McFarland, A. R. (2008). Circumferential-Slot Virtual Impactors with Stable Flow. *Aerosol Sci. Technol*. 42:748–758.

Laucks, M. L., and Twohy, C. H. (1998). Size-Dependent Collection Efficiency of an Airborne Counterflow Virtual Impactor. *Aerosol Sci. Technol*. 28:40–61.

Lin, H., and Heintzenberg, J. (1995). A Theoretical Study of the Counterflow Virtual Impactor. *J. Aerosol Sci.* 26:903–914.

Noone, K. J., Ogren, J. A., Heintzenberg, J., Charlson, R. J., and Covert, D. S. (1988a). Design and Calibration of a Counterflow Virtual Impactor for Sampling of Atmospheric Fog and Cloud Droplets. *Aerosol Sci. Technol.* 8:235–244.

Noone, K. J., Charlson, R. J., Covert, D. S., Ogren, J. A., and Heintzenberg, J. (1988b). Cloud Droplets: Solute Concentration is Size Dependent. *J. Geophys. Res.* 93D:9477–9482.

Noone, K. J., Ogren, J. A., and Heintzenberg, J. (1990). An Examination of Clouds at a Mountain-Top Site in Central Sweden: The Distribution of Solute within Cloud Droplets. *Atmos. Res*. 25:3–15.

Noone, K. B., Noone, K. J., Heintzenberg, J., Strom, J., and Ogren, J. A. (1993). In-Situ Observations of Cirrus Cloud Microphysical Properties Using the Counterflow Virtual Impactor. *J. Atmos. Oceanic. Tech*. 10:294–303.

Ogren, J. A., Heintzenberg, J., and Charlson, R. J. (1985). In-Situ Sampling of Clouds with a Droplet to Aerosol Converter. *Geophys. Res. Lett.* 12:121–124.

Ogren, J., Heintzenberg, J., and Noone, K. (1988). Measurements of the Partitioning of Aerosol Mass and Number Between Cloud Droplets and Interstitial Air. *Annalen der Meteorologie.* 25:34–36.

Richardson, M. S., DeMott, P. J., Kreidenweis, S. M., Cziczo, D. J., Dunlea, E. J., Jimenez, J. L., Thomson, D. S., Ashbaugh, L. L, Borys, R. D., Westphal, D. L., Casuccio, G. S., and Lersch, T. L. (2007). Measurements of Heterogeneous Ice Nuclei in the Western United States in Springtime and Their Relation to Aerosol Characteristics. *J. Geophys. Res.* 112. doi:10.1029/2006JD007500.

Schwarzenböck, A. and Heintzenberg, J. (2000). Cut Size Minimization and Cloud Element Break-Up in a Ground-Based CVI. *J. Aerosol Sci*. 31:477–489.

Twohy, C. H., Schanot, A. J., and Cooper, W. A. (1997). Measurement of Condensed Water Content in Liquid and Ice Clouds Using an Airborne Counterflow Virtual Impactor. *J. Atmos. Oceanic Tech.* 14:197–202.

Twohy, C. H., and Poellot, M. R. (2005). Chemical Characteristics of Ice Residual Nuclei in Anvil Cirrus Clouds: Implications for Ice Formation Processes. *Atmos. Chem. Phys.* 5:3723–3745.

Wieprecht, W., Acker, K., Mertes, S., Collett Jr, J., Jaeschke, W., Brüggeman, E., Möller, D., and Herrman, H. (2005). Cloud Physics and Cloud Water Sampler Comparison During FEBUKO. *Atmos. Environ.* 39(23-24):4267–4277.